

Limits on the Ultra-High Energy Electron Neutrino Flux from the RICE Experiment

I. Kravchenko

Massachusetts Institute of Technology Lab. for Nuclear Science, Cambridge, MA 02139

G. M. Frichter

Florida State University, High Energy Physics, Tallahassee FL 32306-4350

T. Miller*, L. Piccirillo[†], D. Seckel, G. M. Spiczak[‡]

Bartol Research Institute, U. of Delaware, Newark DE 19716

J. Adams, S. Seunarine

*Department of Physics and Astronomy, Private Bag 4800,
U. of Canterbury, Christchurch, New Zealand*

C. Allen, A. Bean, D. Besson,[§] D. J. Box, R. Buniy,[¶] J. Drees, D.
McKay, J. Meyers, L. Perry, J. Ralston, S. Razzaque, D. W. Schmitz**

University of Kansas Dept. of Physics and Astronomy, Lawrence KS 66045-2151

(Dated: November 7, 2018)

* Current address: Applied Physics Laboratory, Johns Hopkins University, Laurel MD

† Current address: Department of Physics and Astronomy Cardiff University Cardiff CF24 3YB United Kingdom

‡ Current address: University of Wisconsin, River Falls, WI 54022

§ Contact: zedlam@ku.edu, for more information on the RICE experiment.

¶ Currently at Vanderbilt University, Nashville, TN, 37235

** Currently at Columbia University, NYC, NY 10027

Abstract

Upper limits are presented on the diffuse flux of ultra-high energy ν_e , based on analysis of data taken by the RICE experiment during August, 2000. The RICE receiver array at South Pole monitors cold ice for radio-wavelength Cherenkov radiation resulting from neutrino-induced in-ice showers. For energies above 1 EeV, RICE is an effective detector of over $15 \text{ km}^3 \text{ sr}$. Potential signal events are separated from backgrounds using vertex location, event reconstruction, and signal shape. These are the first terrestrial limits exploiting the physics of radio Cherenkov emissions from charged-current $\nu_e + N \rightarrow e + N'$ interactions.

I. INTRODUCTION

Neutrinos are generally expected to be an important component of ultra-high energy (UHE) cosmic rays[1]. Neutrinos propagate in straight lines from their source and retain spectral information about their origin - in contrast to protons, electrons or gamma-rays, which interact with cosmic magnetic fields, cosmic radiation backgrounds at microwave and radio frequencies, and material within the source itself. Energies below 100 GeV are the province of solar, supernova and atmospheric neutrino experiments. Above 100 GeV it is expected that astrophysical sources (e.g. AGN, GRBs, the galactic disk) will be observable in planned cubic kilometer scale detectors[2, 3, 4, 5], or perhaps in prototype existing experiments that have pioneered the development of large arrays of optical Cherenkov detectors[6, 7]. Despite their impressive size, even these experiments may be too small to see scientifically interesting fluxes at energies above 10 PeV. Of particular interest, neutrinos of energy 0.1-1 EeV may provide key information for understanding anomalies reported in the cosmic ray spectrum[8, 9, 10] above the “GZK” cutoff[11]. Detection of the nominal flux of GZK neutrinos[12] requires a detector mass equivalent to 100 km³ of water[13]. To achieve such large masses, other techniques have been proposed for this energy range, including detection of horizontal air showers[14, 15, 16, 17], acoustic signals in water or ice[18] and a variety of ideas[19, 20, 21] that rely on detection of radio Cherenkov emission via a process first proposed by Askaryan[22] and recently confirmed in the laboratory[23]. The latter set includes detection of radio pulses generated in the lunar regolith[24, 25], geological salt deposits[26], and Antarctic ice as observed *in situ*[27] or from a high altitude balloon[28]. We report here on the first results from the Radio Ice Cherenkov Experiment (RICE), an array of dipole antennas located in-ice at the South Pole.

The concept behind RICE is illustrated in Figure 1: a neutrino-nucleon interaction results in an electromagnetic cascade, which in turn produces a few nanosecond radio pulse with power concentrated around the Cherenkov angle. Detection of that pulse by several receivers with fast electronics allows for reconstruction of the interaction vertex and the energy/direction of the incident neutrino. Development and status of the RICE experimental configuration is summarized in Section II.

The experiment requires accurate simulation of the expected signal, full calibration of an instrument with many interacting components, and development of techniques for event reconstruction and elimination of spurious backgrounds. Simulation and calibration are discussed in Section III. Additional information concerning our use of numerical techniques to model the Cherenkov signal may be found in Refs. [29, 30]. Calibration of the RICE experiment is described in greater detail in Ref. [31].

Event reconstruction (Section IV) is important not only for the eventual analysis of neutrino observations, but also as a tool for separation of neutrino events from backgrounds. Background events result from either correlated or uncorrelated receiver hits. The former are due to impulsive transients associated with human activity in and around South Pole station[32]. Uncorrelated receiver hits result from thermal noise in the ice. The presence of continuous wave transmissions is readily detected, and is accounted for in the data analysis. Related issues are discussed in Section V.

In development since 1995, the bulk of RICE operations has been devoted to calibration,

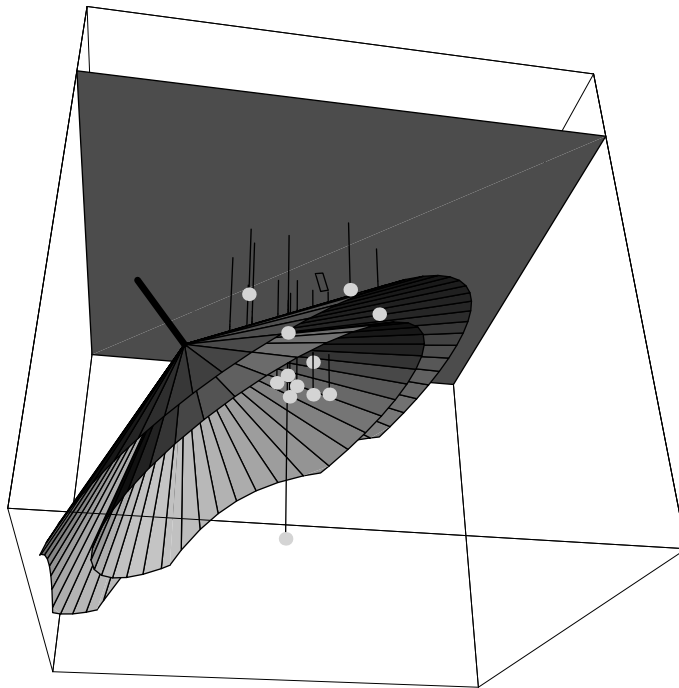


FIG. 1: RICE concept. The RICE array (viewed from below) is drawn schematically to scale, showing cables and antenna locations. The small rectangle on the surface is the Martin A. Pomerantz Observatory (MAPO) which houses the RICE electronics. An electron neutrino is incident from above the horizon and interacts in the ice. An electromagnetic shower (hidden) results, which in turn generates an outgoing cone of radio Cherenkov radiation. Two cones, drawn at $\theta_c \pm 3^\circ$, depict an approximate 3 dB range of signal strength.

understanding backgrounds, and developing strategies for dealing with those backgrounds. As a result, the experimental configuration has been dynamic - a situation which complicates both data-taking and analysis. We therefore chose to “freeze” the configuration for one month (August 2000), take data, and analyze the results. The analysis of August 2000 data is presented in Section VI. Refinement of the techniques used in the present analysis has been an ongoing process. As such, the present analysis is more complete than the preliminary analysis presented in Ref. [33] and our present limit is somewhat stronger, although based on the same data.

Limited to a single month of data, the exposure analysed here is too short to provide a significant likelihood of finding actual neutrino events, at least given theoretical predictions. Our current search yields a null result, and we use it to place upper limits on proposed theoretical models. Accordingly, we have taken a conservative approach throughout our analysis, generally choosing simpler options when confronted with choices in the analysis, often resulting in a less restrictive limit. We present a broad survey of systematic uncertainties in Section VII.

RICE was originally conceived as an experiment to search for electron neutrinos via charged current interactions and the subsequent electromagnetic showers. Since these are reasonably well studied, the signal predictions are fairly robust and these events remain the primary subject of the current paper. It is understood, however, that at energies well in excess of 1 PeV, LPM effects reduce the efficiency for detecting electromagnetic showers. As a result, hadronic recoil showers, which are produced by neutrinos of all flavors in both charged and neutral currents, may be important for detection of neutrinos at the highest energies. Section VII includes a discussion of the efficiency for RICE to detect neutrinos via hadronic showers.

Finally, we summarize our discussion in Section VIII and consider possible future applications of the radio technique at the South Pole.

II. OVERVIEW OF RICE

During August 2000, the RICE experiment consisted of a 16-channel array of dipole radio receivers (“Rx”), deployed within a 200 m×200 m×200 m cube, at 100-300 m depths. The 10-cm fat dipole antennas were designed both to produce a peak response at 250 MHz (compatible with our expected signal and the rest of the DAQ), and to allow piggyback deployment in holes drilled for the AMANDA experiment. Signals from each antenna are boosted by an in-ice amplifier (36 dB), carried by coaxial cable to the surface observatory, filtered to suppress noise below 200 MHz, re-amplified (52 or 60 dB), and fed into a CAMAC crate. The gain of the in-ice amplifier is chosen so as to allow measurement of the in-ice radio background ($T_N \sim 250\text{K}$), after transmission over the co-axial cable. The gain of the surface amplifier is chosen to bring the in-ice thermal background and expected signals within the dynamic range of the DAQ electronics. The amplifiers are adjusted for each channel so as to reduce the channel-to-channel variation in receiver response. The 200 MHz filter effectively eliminates low frequency incoherent galactic radio noise, and an impulsive background generated by AMANDA phototubes which peaks below 50 MHz. The RICE experimental bandpass is effectively $\Delta f \approx 200 - 500$ MHz.

After entering the CAMAC crate, the signals are split, one copy being sent to a bank of 4 digital oscilloscopes, and the other going to trigger logic. The trigger requires a four-fold coincidence within a 1.2 μs window, four hits being required to perform event reconstruction. A common discriminator threshold is adjusted to maintain a trigger rate that permits monitoring of backgrounds without a significant reduction in livetime for true neutrino events. For most event geometries, the 1.2 μs window accomodates signals propagating across the array and along cables of differing length to reach the surface DAQ.

In the event of a trigger, times for each channel to cross the discriminator threshold are recorded by a TDC module in the DAQ. These times form the basis for an on-line software veto designed to reject noise events resulting from surface activity. Events passing the veto are recorded with 8 μs of waveform data per channel transferred from the scope and saved on disk for later analysis. The waveform data is critical to understanding the background environment, the nature of noise events, and provides the event timing used for performing event reconstruction.

In addition to the receivers, four antennas are configured and deployed as in-ice transmitters for use as calibration sources. Three horn antennas are deployed on the surface, and provide a further veto of surface activity. More details of the DAQ and trigger configuration can be found in [31].

III. THE RICE SIGNAL PATH

The neutrino detection efficiency is determined by a detailed Monte Carlo simulation of the RICE experiment, which naturally divides into four stages: 1) the incident neutrino flux and the neutrino-nucleon interactions, 2) generation of the subsequent electromagnetic shower and the radio signal from that shower, 3) propagation of the radio signal through the ice, resulting in an electric field $\vec{E}_i(t)$ at the input to the i^{th} antenna, and 4) response of each antenna, and conversion to an input voltage $V_i(t)$ for each channel received by the DAQ hardware.

The primary result of the Monte Carlo is an energy-dependent effective volume for detection of electron neutrinos which undergo charged current scattering from nucleons in ice and so create an electromagnetic shower. For a given model spectrum and integrated livetime, the expected number of detections is then readily determined. We compare this with the observed number of detections, and obtain an upper limit to the normalization of the model spectrum.

A. Shower Production Rate

The simulation assumes electron neutrinos of energy E_ν are incident isotropically from the *upper hemisphere*. The upward neutrino flux is negligible due to the high opacity of the Earth for $E_\nu > 1$ PeV[34]. Events are distributed uniformly over a cylindrical volume with a depth and radius large enough to contain the most distant detectable events for a given neutrino energy. The design energy and angular range of the RICE search, as well as the neutrino flavor, all differ from those of lower energy cosmic neutrino experiments, which primarily search for upward-going muons.

The probability of a charged current interaction within the Antarctic ice is determined using the cross-sections of Gandhi et al.[35]. Other extrapolations of Standard Model cross-sections to the high energy range differ by as much as 20% at 10 EeV[36, 37, 38, 39]. For oxygen, the per-nucleon cross-section is reduced due to nuclear structure effects[40, 41] by 12%(1 PeV) to 24%(100 EeV)[42, 43]. The electromagnetic shower energy is related to the neutrino energy by the inelasticity, $E_s = (1 - y)E_\nu$. We select y randomly from $d\sigma/dy$, also taken from Ref. [35]. The mean value of y drops from 26% to 20% as the neutrino energy increases from 1 PeV to 100 EeV.

RICE sensitivity to hadronic showers is discussed in Section VII. Hadronic showers may be produced by either charged or neutral current interactions. Neutral current cross-sections were also taken from Gandhi et al., and similarly modified for nuclear effects. At energies above a PeV, the cross-sections are dominated by sea-quarks and so, a) the $\bar{\nu}$ cross-sections

are nearly equal to the ν cross-sections, b) the neutral current cross-sections are nearly 0.5 times the charged current cross-sections, and c) the $d\sigma/dy$ distributions are nearly identical for all interaction types.

The energy in hadronic showers evolves into an electromagnetic shower as π^0 mesons in the shower decay to two photons. This process is suppressed for $E_{\pi^0} \gtrsim 6$ PeV, because the rate for hadronic interactions of π^0 's exceeds the time dilated decay rate. As a result, conversion of hadronic energy to electromagnetic energy is postponed until average particle energies are below a few PeV, with the consequence that hadronic showers do not suffer greatly from LPM effects[44]. In our later discussion we include hadronic showers as electromagnetic showers with energy $E_s = yE_\nu$ and discount any LPM effects.

B. Expected Signal Strength due to an Electromagnetic Shower

The coherent emission of radio-frequency Cherenkov radiation from cascades has been discussed by several authors[27, 29, 30, 44, 45, 46, 47, 48, 49, 50]. Laboratory measurements directly probe the coherence and have verified a linear scaling of the field strength with shower energy[23], but a precise determination of signal strength for showers developing in ice still requires numerical simulation.

The most recent papers compare radiation from showers produced using the GEANT particle physics and detector Monte Carlo package with codes that are derivatives of the pioneering work of Zas, Halzen and Stanev[45] (ZHS). Razzaque et al.[29] used GEANT 3.21 and found that emission from showers with energies of 0.1-1 TeV was typically 30% lower than in ZHS at frequencies $f < 500$ MHz, the regime for fully coherent emission from the shower. Subsequently, Alvarez-Muñiz et al.[50] showed that the low result from GEANT 3.21 was due to an approximation made in the tracking of low energy electrons. Utilizing an optional tracking algorithm, or switching to GEANT 4, produced results only 10% smaller than the ZHS code. This result has been confirmed by Razzaque et al.[30], who also show that other characteristics of the radio pulse are not greatly affected by the change in GEANT configuration.

In addition to overall normalization, the frequency spectrum (and phase) convolved with the experimental bandwidth determines the detected signal strength. For both the GEANT and ZHS codes the power spectrum increases with frequency until $f \sim 1$ GHz. At higher frequency the ZHS code produces a spectrum which flattens and then decreases in the multi-GHz range[45, 48], whereas the spectrum from the GEANT code remains flat for $f > 1$ GHz[29]. These differences are still being studied, but are relatively unimportant for RICE, where propagation in ice, antenna response, cable losses, and noise filters reduce the effective bandwidth to the range $\Delta f \approx 200 - 500$ MHz[31].

The angular radiation pattern is mainly determined by the length of the shower, for which the GEANT and ZHS codes are in agreement at energies of 100 GeV[29]. However, the peak of the RICE energy response is some 6 orders of magnitude higher, so an extrapolation from low- to high-energy must be performed. Accordingly, we include the modest lengthening of the shower when extrapolating from 1 TeV to 1 PeV[51], and for electromagnetic shower energies above one PeV the radiation pattern is adjusted to include LPM effects[46, 47].

Given these considerations, for our Monte Carlo simulation we use a radio pulse with spectral form taken from the original ZHS paper, but with a normalization given by the most recent GEANT studies and an angular pattern which includes shower evolution and LPM effects. We estimate that the potential systematic error in this procedure is of order 10% for an average shower. We do not model shower-to-shower fluctuations, nor do we include the near zone corrections to the radiation pattern[49] that may be important for impact parameters of a few hundred meters.

For our later discussions, we approximate hadronic showers as electromagnetic showers of the same energy, but with LPM effects turned off. This approximation ignores modest differences in the longitudinal development of the shower due to its hadronic nature. In the case of combined electron induced and hadronic showers, due to the different longitudinal development, the two pulses may not add coherently at all observation angles. Thus, we approximate the two pulses as distinct objects and evaluate their detectability separately. This procedure will sometimes result in double counting an event, and in other cases will miss events where neither shower would trigger RICE by itself, but the combined showers would.

C. Propagation through Polar Ice

Radio propagation in ice[52] is described by a complex dielectric constant ϵ , which in principle is a function of the density, temperature, composition, and crystalline structure of the ice, as well as the frequency and polarization of the radio wave. The real part of ϵ defines the index of refraction n_{ice} and depends primarily on density, while the complex part of ϵ is related to absorption or, equivalently, the attenuation of field strength. We use an index of refraction $n_{ice} = 1 + 0.84\rho$, where $\rho(z)$ is the ice density in g/cm^3 , which yields $n_{ice} = 1.3$ near the surface and a deep ice value of 1.78. The ice is assumed to be free of discontinuities. The attenuation length is taken to be frequency and temperature dependent. (Note: we work with the field attenuation length, which is twice the power absorption length.)

We have searched for “echoes” in transmitter data indicative of reflections from interfaces in the ice or from the surface, but have found no evidence for such an effect. Surface events do show evidence for “double pulses”, but the time separation is typically independent of receiver channel, showing that the double pulses are properties of the source and not features of the propagation. Data from nadir looking synthetic aperture radar suggest that variations of n_{ice} at internal interfaces in the ice are quite weak, generating reflected waves down by 20-90 dB relative to the wave transmitted through the interface[53]. Non-stratified variations in n_{ice} may lead to incoherent scattering, a loss of signal strength, and a delayed clutter of scattered waves. We see no evidence for such effects in our buried transmitter data.

Figure 2 shows two models for $\lambda(\nu, T)$, the frequency and temperature dependent attenuation length. The current analysis makes use of a parameterization due to Provorov[54]. We have also constructed a model combining high frequency data ($\nu > 5$ GHz) taken with pure polycrystalline ice in the laboratory[55], with low frequency measurements ($\nu < 600$ MHz) taken on a sample of glacial ice from Greenland[56]. The two models differ by less than a factor of two in the RICE bandpass of 200-500 MHz. Although there is agreement between

these two models, other measurements of attenuation at 300 MHz vary significantly. Extrapolation of Debye spectra measured for pure ice at lower frequencies[57, 58] yield attenuation lengths more than an order of magnitude longer at -50 C, while data from a sample taken in Little America[52] indicate λ a factor of 3 smaller at -40 C. We speculate that the differences are due to varying levels of impurities affecting the number of charge carriers that contribute to conduction at low frequency[58, 59]. The ice at South Pole should be relatively impurity-free due to its remote location and isolation from wind-borne sea salts. Attempts to measure the attenuation length directly using the RICE array were unsuccessful, primarily because the attenuation length in the RICE bandpass exceeds one km, far beyond the size of the array and its buried transmitter-receiver pairs.

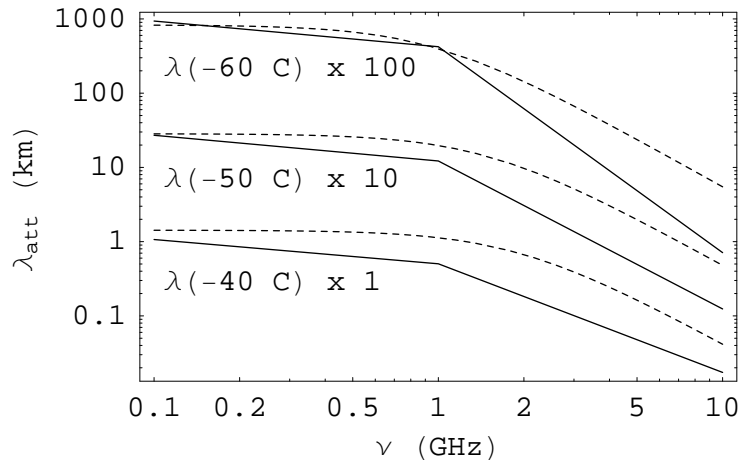


FIG. 2: Models for attenuation length, $\lambda_{att}(\nu, T)$ at three temperatures. Solid curves are for a parameterization due to Provorov[54]. Dashed curves are for a model combining data from Matsuoka, Fujita and Mae[55], and Westphal[56]. The pairs of curves are offset for visibility.

D. From Antenna to Trigger

Knowing the amplitude and timing response of the RICE receiver array is crucial to determining the sensitivity for neutrino events, as well as the ability to reconstruct events and reject spurious backgrounds. Both these calibrations are most easily analyzed in the frequency domain - transforming back to the time domain only as the signal enters the DAQ (trigger logic and oscilloscopes). The signal incident to the DAQ is given by

$$V_o(\nu) = T(\nu)V_i(\nu), \quad (1)$$

where T is the transfer function and V_i is the voltage generated on the antenna. For a dipole antenna with effective height \vec{h} , the input voltage is given $V_i = \vec{h} \cdot \vec{E}(\nu)$, where $\vec{E}(\nu)$ is the electric field vector of the Cherenkov signal. The transfer function to pass signals through

to the DAQ is given by

$$T(\nu) = A(\nu) \frac{Z_{ant}}{Z_{ant} + Z_{cable}}, \quad (2)$$

where $A(\nu) = A_1 C A_2 F / \sqrt{2}$ is a product of terms to account for the amplifiers (A_1 and A_2), cable losses (C), the 200 MHz filter (F) and the splitter, $Z_{cable} = 50\Omega$, and $Z_{ant}(\nu)$ is the frequency dependent antenna impedance.

The University of Kansas Antenna Testing Range has been used both to measure the effective height for RICE antennas and to confirm a basic dipole antenna pattern. Amplifier gains are measured *in situ*. Cable losses and the effects of filters and splitters are measured in the lab. The full frequency response is then tested using continuous wave transmissions from the in-ice transmitters. The model reproduces the shape and normalization of data, with errors no greater than ± 3 dB in voltage, antenna-by-antenna, across the frequency spectrum[31].

After the signal arrives at the DAQ, the Monte Carlo simulates the RICE trigger by transforming the signal back to the time domain, comparing to the relevant discriminator thresholds and checking for a 4-fold coincidence within $1.2 \mu\text{sec}$. Sample results are shown in Figure 3.

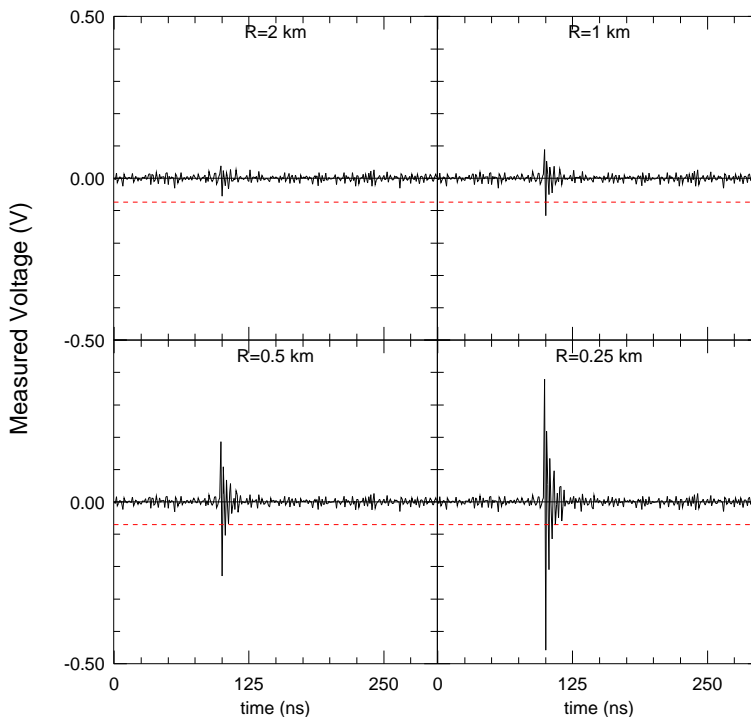


FIG. 3: Voltage as a function of time expected for a 10 PeV cascade at different distances from a typical RICE receiver. The receiver is positioned on the Cherenkov cone with its dipole axis aligned along the electric field. The noise background is sampled from actual data. The horizontal dashed line is the ‘ $5 - \sigma$ ’ threshold used in analysis.

Details of the antenna array and DAQ also influence the timing accuracy, critical for

event reconstruction. A fairly straight forward survey of signal delays within the cables and DAQ electronics indicates that these contribute $< 5\text{ns}$ to the timing uncertainty[31]. Uncertainty in antenna positions is more important, $\sim 4\text{ m}$ or 20 ns . A more subtle issue is consistently determining an arrival time from the pulse waveform. In Figure 3 one observes a characteristic ringing of our antennas at approximately 300 MHz , and damped with a time constant of order 10 ns . Still, the leading edge of the pulse can be resolved to a few ns on an event-by-event basis. Pulse shapes for noise events originating from the surface are not as clean or reproducible, particularly for high-amplitude signals which saturate the amplifiers, and an arrival time uncertainty of 50 ns is more typical. For tests involving the in-ice transmitters, the pulses are reproducible, but the impulse is considerably broader than for a neutrino event. We expect that strong neutrino pulses can be consistently timed to $< 2\text{ ns}$, but weaker pulses give uncertainties of order 10 ns .

E. Effective Volume

We define the effective volume of the array for shower detection by

$$V_{eff}(E_s) = \frac{1}{2\pi\tau} \int \epsilon(E_s, \vec{r}, \hat{n}, t) d\vec{r} d\Omega dt, \quad (3)$$

where $\epsilon(E_s, \vec{r}, \hat{n}, t)$ is the efficiency for detection of an electromagnetic shower of energy E_s , at position \vec{r} , and direction \hat{n} . We normalize V_{eff} to $2\pi\text{ sr}$ to account for the solid angle of the incident beam and average over the exposure time τ since ϵ depends on adjustable DAQ settings.

Figure 4 illustrates ϵ for showers with $E_s = 1\text{ EeV}$. At small radial distances, downward showers initiated below the array are not detected since the Cherenkov cone does not intercept the array. At modest distances, the efficiency is limited by the width of the Cherenkov cone. At large distances, attenuation in the ice limits the horizon of the detector. Most of the efficiency is in the upper km of ice, since the ice warms with depth and the effects of attenuation increase. Averaged over depth, the efficiency for this exposure is a maximum of about 3% from $1\text{-}2\text{ km}$, and is less than 0.3% for $r > 4\text{ km}$.

The effective volume averaged over the August 2000 exposure is shown as the bold curve in Figure 5. For $E_s = 300\text{ PeV}$, V_{eff} is $\sim 1\text{ km}^3$. For energies below about 50 PeV , $V_{eff} \sim E^3$ [27], reflecting the nearly linear scaling of the signal strength with shower energy. Above 50 PeV three effects become important as the range for signal detection increases: a) the target volume becomes more and more disk-like, so that $V_{eff} \sim E^2$, b) eventually attenuation dominates so that $V_{eff} \sim \ln(E)^2$, and c) LPM effects narrow the thickness of the Cherenkov cone, further reducing V_{eff} .

Figure 5 also illustrates two complementary contributions to uncertainty in the analysis. Any variation in the attenuation length is most important at high energies, where the array is probing distances well over 1 km . Variations in signal strength, however, are most important for energies below 100 PeV . The latter regime is also most sensitive to calibration of receiver sensitivities and changes in the discriminator threshold or trigger conditions. For

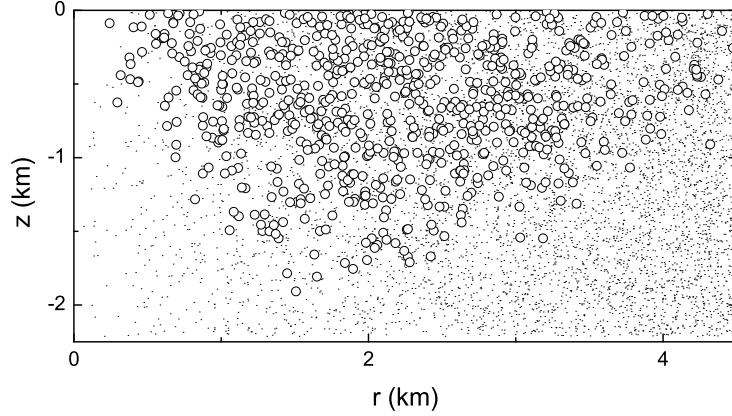


FIG. 4: Radial and depth distribution for 60000 Monte Carlo events at shower energy of 1 EeV. The Monte Carlo exposure is even in depth, unit area and solid angle above the horizon. Black dots show event vertices for 10% of the simulated events. Open circles indicate the positions of simulated events which would result in RICE triggers.

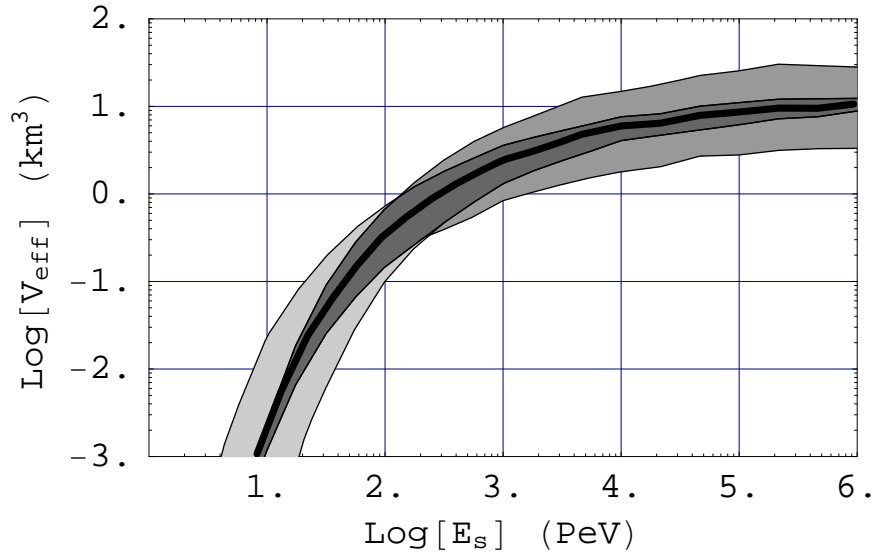


FIG. 5: RICE effective volume (Eq. 3), as a function of shower energy, for the August 2000 configuration. The nominal result corresponds to the bold curve. The region in medium gray spans variations in response due to variation in the attenuation length by factors of (0.5-2.0). The region in light gray shows the range due to changes in signal strength by (0.5-2.0). The region shaded in dark gray is within the range of both variations.

example, changing the trigger requirement to a 5-fold multiplicity, increasing the discriminator threshold by 25%, or decreasing the signal strength by a similar amount, all have approximately the same effect on V_{eff} .

IV. EVENT RECONSTRUCTION

Event reconstruction is performed in two stages: 1) an event vertex is determined based on pulse timing and 2) neutrino direction and shower energy are determined from fitting a Cherenkov cone to the signal amplitudes in channels registering hits.

Techniques for vertex reconstruction were developed using short duration in-ice transmitter pulses broadcast to the receiver array[31]. Given measured time differences δt_{ij} between all pairs (i, j) of hit antennas, we perform a χ^2 minimization to reconstruct the source location. A typical transmitter calibration event is displayed in Figure 6. The relevant time scales are evident. Compared to the dimensions of the array, the pulses are well resolved. Although the pulses themselves extend over ~ 50 ns, the pulse shapes are repeatable with arrival times determined to better than 2 ns rms. Combining uncertainties due to in-ice propagation, surveyed positions of the receivers, propagation delays through the array cables and electronics, and pulse time resolution, we infer a precision for determining transmitter positions of better than 5 m, corresponding to a time resolution of ~ 25 ns.

The same techniques are used for analysis of live data and to discriminate between potential signal events and various backgrounds. The vertex reconstruction is underdetermined for three or fewer hits, so we require four hits to form a trigger. With four hits, a geometrical reconstruction typically admits either a unique solution or no solution at all. Thus, for a point source event $\chi^2 \rightarrow 0$, whereas for any finite χ^2 a valid vertex reconstruction is not possible. With five or more hits, a valid reconstruction should yield a $\chi^2/\text{d.o.f.}$ of order 1.

To discriminate against surface noise, a timing uncertainty $\delta t \sim 50$ ns is appropriate due to the uncertain nature of the pulse shapes. For vertices within the array boundaries or nearby on the surface, we reconstruct positions to roughly 10 m accuracy - sufficient to distinguish surface events from in-ice neutrino candidates.

For reconstruction of neutrino event candidates, a smaller $\delta t \sim 25$ ns is dominated by uncertainty in receiver positions. More generally, for events within a km of the array we obtain vertex location resolutions of $\sim 0.1 R$, where R is the distance from the vertex to array center. Radial distance is not well determined beyond 1 km, where the timing accuracy does not allow one to distinguish between a spherical wavefront and a plane wave.

We utilize the relative signal amplitudes amongst the hit antennas to determine the section of the Cherenkov cone detected and, hence, the direction of the incident neutrino. The difference between true and reconstructed sky position is less than ~ 10 degrees for half of the simulated neutrino events. Similarly, the energy resolution for showers at 100 PeV is $\Delta E/E \sim 0.5$ for those cases where the Cherenkov geometry is well-determined[31].

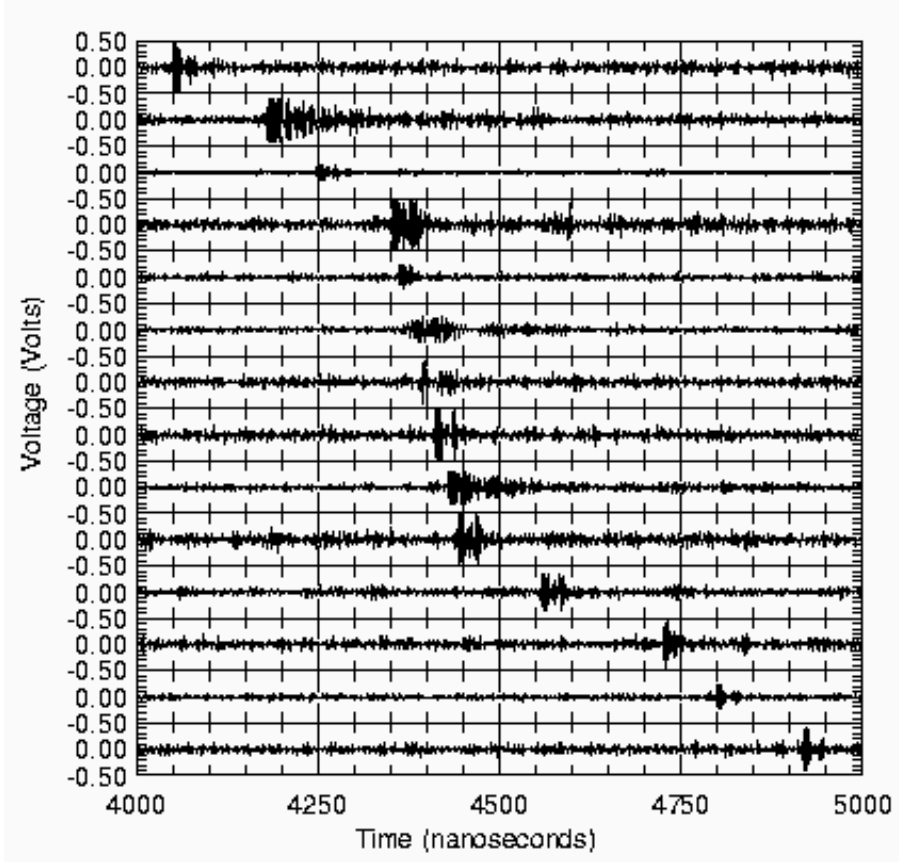


FIG. 6: Voltage traces for a calibration event in which a 5 ns square pulse is sent down cable to an in-ice transmitter and broadcast to the array. Cable losses and bandwidth limitations of the transmitting antenna broaden the time structure of the pulse significantly. Receiver channels are ordered (from top to bottom) in order of the modeled time delay between the pulse transmission and reception in the DAQ. There are only 14 traces in the figure as two oscilloscope channels were dedicated to triggering in this test.

V. BACKGROUNDS AND FILTERS

The radio environment at South Pole includes both a thermal background and a variety of anthropogenic effects[32]. The 200 MHz high pass filter eliminates low frequency backgrounds before signals reach the DAQ. Data-taking is inhibited while the station satellite link (303 MHz) is operating. Still, the raw RICE trigger rate is dominated by electronics noise generated on the surface, mostly in or nearby MAPO. These events can be readily eliminated by a sequence of criteria based on the reconstructed vertex location and the quality of the event pulse shape, as detailed in the filter and analysis chain given below.

Thermal noise fluctuations represent an irreducible background even after all impulsive human activity has been eliminated. Each receiver is characterized by a measured effective

noise temperature $T_n \sim 250 - 300$ K, which includes the ambient radiation field, the physical temperature of the antenna, and the noise generated by the in-ice amplifier. The thermal noise contribution to V_i in Eq. 1 is given by

$$V_{rms} = (k_B Z_{cable} T_n \Delta\nu)^{1/2}, \quad (4)$$

where the effective bandwidth $\Delta\nu$ is limited by cable losses, the filter, and by either the oscilloscope or the discriminator. The primary mechanism for reducing thermal noise is to require an $n - \text{hit} \times m - \sigma$ trigger, within the $1.2 \mu\text{s}$ coincidence window, where σ is the corresponding noise contribution to the voltage as seen by a particular DAQ channel. With 4-hits required for event reconstruction, a $5 - \sigma$ threshold gives an expected rate of order 10^{-5} Hz. As a practical matter, the discriminator threshold is set at a level which corresponds to roughly $4 - \sigma$ as recorded by the oscilloscope; however, the bandwidth for the discriminator is somewhat less than that of the oscilloscope and thermal fluctuations do not strongly influence the trigger rate.

During event analysis we apply various cuts based on the waveform data to eliminate any remaining ‘‘thermal’’ triggers. In addition to the $n - \text{hit} \times m - \sigma$ criterion, one can discriminate against such events on the basis of vertex location, as shown in Figure 7. Events where uncorrelated noise results in the production of four random hits within $1.2 \mu\text{s}$ tend to reconstruct within the array, whereas most of our source models are dominated by events at a distance of several km. Additionally, events from uncorrelated noise typically do not give good fits to a Cherenkov cone.

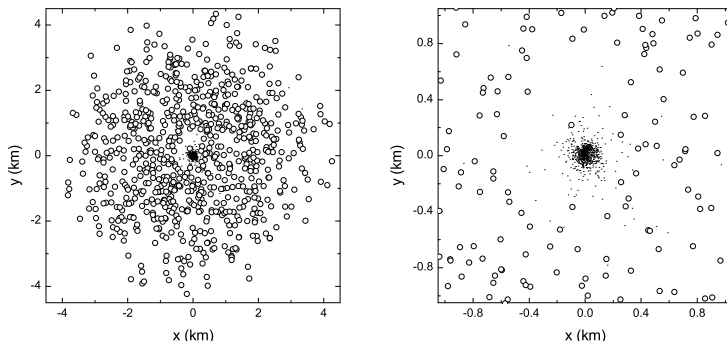


FIG. 7: Lateral distribution of Monte Carlo events for 1 EeV showers (open circles) as compared to the vertex position constructed for events due to 4 uncorrelated noise hits (dots). The latter predominantly lie within the array boundaries, whereas true neutrino events do not. The deficit of neutrino events in the inner ~ 0.5 km reflects the same geometric exclusion illustrated in Fig. 4. Left panel: all events. Right panel: inner kilometer. There are 778 points in each sample.

Given the high threshold, RICE does not have a naturally occurring source of impulsive backgrounds that would obscure the neutrino induced signals. For example, catastrophic dE/dX from ultra high energy muons could mimic a neutrino event, but the rate for this process is expected to be less than 0.1 event per yr[60], and generically is smaller than the

neutrino detection rates. Although this implies that RICE is essentially a signal limited experiment, it also means that there is no naturally occurring source which may be used to calibrate the experiment.

The full filter and analysis chain used to separate candidate neutrino events from impulsive and thermal backgrounds consists of the following steps.

- *On-line filter*: The majority ($> 99\%$) of events originating from the surface are eliminated by a software algorithm based on pairwise timing correlations. The algorithm, which uses the TDC times recorded for each channel containing a hit, takes ~ 25 ms to execute. Events which would vertex in the ice pass with high efficiency. Events which pass this software filter have waveforms read out from the digital oscilloscopes for further analysis.
- *Elimination of CW frequencies*: Waveforms are transformed to the frequency domain, scanned for lines, filtered, and transformed back to the time domain.
- *Scanning for 5σ fluctuations*: The first μ s of each waveform is used to evaluate the ambient background noise level for that channel. As these are consistent with in-ice thermal noise, it forms a physical basis for calibrating the signal strength in hit channels. The remainder of the waveform is scanned for well separated 5σ excursions. A list of pulses for each waveform is generated.
- *Double-pulse elimination*: Many surface events contain channels with multiple pulses, which may allow such events to pass the on-line filter. Events with multiple pulses in a single channel are rejected.
- *4-fold 5σ criteria*: Four hits must occur within 1.2μ s.
- *Vertex reconstruction*: We require that the hits admit to an acceptably well-fit vertex. With four hits, this is a simple yes/no decision based on the reconstruction χ^2 . For events with five or more hits, if χ^2 is good the event is accepted. If χ^2 is large, the vertex reconstruction is recalculated after elimination of any one hit, allowing for the possibility that a chance noise hit is captured at the same time as a neutrino event. With 8000 samples and a $5-\sigma$ threshold, we estimate a chance occupancy of $\sim 4 \times 10^{-3}$ per channel, or somewhat less than 7% probability of contamination per event. If the new χ^2 is also large, the process is iterated until either χ^2 is acceptable or the event contains less than 4 hits, at which point it is rejected.
- $z < -50 \text{ m}$: The reconstructed vertex is required to be at least 50 m below the ice surface.
- *Hand Scanning*: Remaining events are scanned, by eye, for patterns or defects.
- *Event reconstruction*: Each event is tested against the hypothesis that the hits are due to a Cherenkov cone radiation pattern from the reconstructed vertex. The cone constructions are analyzed by hand to ensure that acceptance/rejection is robust.

- *Waveform quality*: The waveforms are compared to simulated waveforms (e.g. Figure 3) to ensure that the time structures of the recorded signals are consistent with model predictions.

The detector Monte Carlo simulation has been used to test the filter and analysis sequence. Simulated neutrino events which contribute to V_{eff} pass the on-line filter with $80 \pm 5\%$ efficiency. The remaining stages pass simulated events with $85 \pm 5\%$ efficiency. These factors are not included in V_{eff} shown in Figure 5, but are included in subsequent calculations of event rates and limits.

VI. ANALYSIS OF AUGUST, 2000 DATA

During August 2000, the RICE experiment was operated in a stable configuration for a total of 660.1 hrs. Data-taking was suppressed while the South Pole Station satellite link was operational (~ 242 hrs). Additional dead time accrued during the execution of the on-line filter algorithm (~ 35 hrs), during the readout of events which passed the on-line filters (~ 27 hrs), and during readout of unbiased events and a sample of vetoed events taken for monitoring purposes (~ 23 hr). All told, the exposure was 333.3 hrs of livetime.

Table I summarizes the number of hardware triggers and the success with which they pass our various filter criteria. Evidently, the trigger rate is dominated by surface-generated transient noise backgrounds. The on-line filter successfully removes 99.8% of these in real time. Of the remainder, only 0.2% pass automatic scanning procedures, leaving just 22 events to be looked at by hand. Of the 22 events scanned by trained physicists, 11 exhibited

Total triggers	5,058,976
On line filter	9,442
$4 \times 5\sigma$ cut	73
double-pulse, $Z < 50\text{m}$	22
defect and pattern checks	1
Cherenkov cone test and waveform quality	0

TABLE I: Summary of analysis of August, 2000 data.

one of three repeated patterns of antenna hits and relative times, indicating a man-made source. Another 7 had multiple pulses, but with significant activity in the first microsecond of waveform data which may have defeated the automated double-pulse filter. Three events, all occurring on the same day, had pulses only at the tails of the waveforms, indicative of a significant spectral correction for a transient continuous wave transmission. One event remained, which was subjected to further analysis.

The pattern of antenna hits failed the test for consistency with a Cherenkov-cone originating from the pre-determined vertex: $\chi^2/\text{d.o.f.} > 1000$. Upon examination, the event had four hits that were nearly coplanar, with two hits on one side of the array and the other

two nearly opposite, while the event reconstruction puts the vertex nearly on the same plane and in the middle of the array. This configuration cannot be fit to a Cherenkov cone. The pulshapes were checked for consistency with neutrino generated signals. They were somewhat broad in this regard, 50-200 ns depending on the observers definition, but significantly wider than the features evident in Figure 3. Finally, the location of the vertex in the center of the array is consistent with an interpretation where the multiple hit event arises from uncorrelated signals in the individual channels, whereas for the model neutrino spectra we considered, the event vertices lie well outside the array boundaries (see Figure 7). Based on these considerations, we conclude that there were no neutrino events in the August 2000 data sample.

Given the total livetime for the August, 2000 dataset, the effective volume, and the efficiency for events to pass our filters, we calculate a 95% confidence level upper limit on the incident ν_e flux for several theoretical models, as shown in Figure 8. The limit is derived by first calculating the expected number of events during the August 2000 exposure for a given model, and then adjusting the model flux by a normalization factor so that the expected number of events would be 3.0, the 95% c.l. bound for zero events and negligible background. The limit curves in the Figure then replicate the shape of the test spectrum at an amplitude corresponding to the limit. Generally, the limits from the current analysis are some 2-3 orders of magnitude above model predictions.

Alternatively, Figure 9 shows upper limits assuming an incident power law neutrino energy spectrum: $dN/dE_\nu \sim E^{-\gamma}$. Again, with no events, the Figure is intended to show limits on the normalization of the spectrum over the energy range which gives the greatest contribution to the rate. As the spectral index increases, the sensitive region is pushed to lower energy.

VII. DISCUSSION

The search for ultra high energy neutrinos described in this paper yields zero signal candidates. Given the prototype nature of the current RICE deployment and the limited exposure used for the present analysis, this is not an entirely unexpected result. Accordingly, our discussion is focussed on the uncertainties that go into our analysis and on relaxing the limitations we imposed on the event types and geometry we consider.

A. Uncertainties

Potential systematic uncertainties are summarized in Table II. The Table is organized along the same lines as the discussion in Section III, where a detailed description of input to our Monte Carlo is described. Quoted uncertainties refer to particular quantities, not how they propagate through to an uncertainty in limits on any specific flux model.

Uncertainties in neutrino nucleon cross-sections reflect differences among available standard model perturbative QCD calculations. Similarly, uncertainties in shower simulations and signal generation reflect differences between GEANT 4 and ZHS simulations. A discussion of LPM issues is given below and leads into the discussion of hadronic showers and

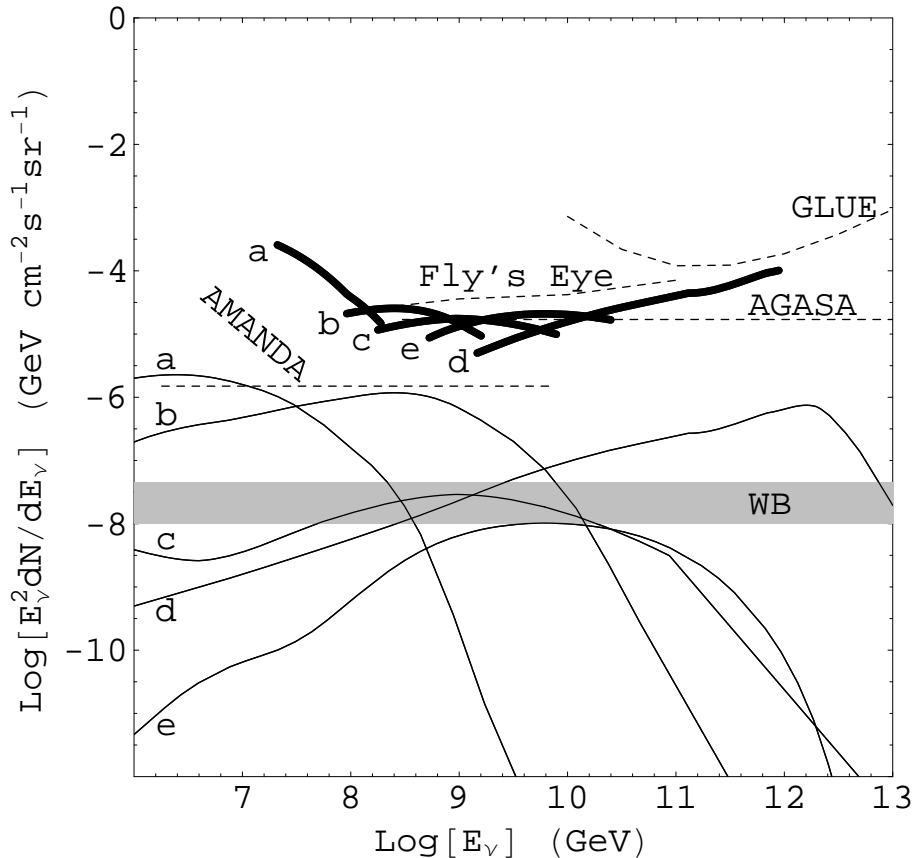


FIG. 8: Neutrino flux model predictions (thin) and corresponding RICE upper limits (95% confidence level; thick), as a function of neutrino energy. The predictions and RICE limits correspond to (a) Stecker & Salamon[61] (AGN), (b) Protheroe[62] (AGN), (c) Mannheim[63] model A (AGN), (d) Protheroe & Stanev[64] (topological defect), (e) Engel, Seckel & Stanev[13] (GZK-model). Each segment corresponds to the neutrino energy range responsible for the middle 80% of the event rate. Results from AGASA[65] (assumed E^{-2} spectrum for $E_\nu > 3 \times 10^8$ GeV), GLUE[25], Fly's Eye[66] (derived using $\sigma_{\nu N}$ from Ref. [35]), and AMANDA[67] are shown as dashed lines. The gray bar (WB) shows the range of upper limits derived by Waxman and Bahcall[68] under differing assumptions about the cosmological evolution of UHE cosmic ray sources.

other event types. A complete understanding of attenuation in polar ice is still lacking. The rough factor of two quoted in the table is based on the considerations discussed in Section III C. The 3 dB uncertainty in channel response is taken from Ref. [31], as are estimates of timing resolution and our ability to reconstruct vertex location. Uncertainties for the on-line filter and off-line analysis efficiencies are based on Monte Carlo studies.

The largest uncertainties concern the attenuation in ice at frequencies of order 300 MHz and the channel-to-channel calibration of the receivers, as summarized by the gray bands in

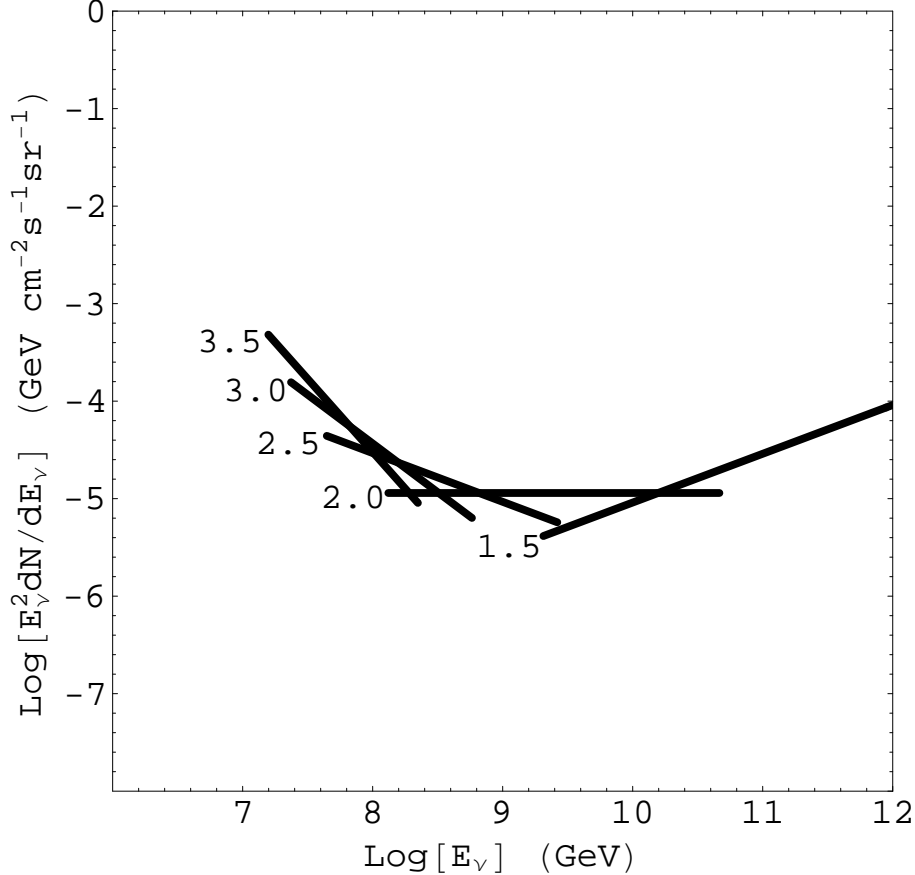


FIG. 9: RICE upper limits (95% confidence level) on neutrino flux assuming a $dN/dE \sim E^{-\gamma}$ input spectrum, with the spectral index taking on values of $\gamma=1.5, 2.0, 2.5, 3.0, 3.5$.

Figure 5. Uncertainties in calibration of signal strength or receiver sensitivity directly affect the threshold for RICE, but do not greatly alter the effective volume for shower energies above 1 EeV. This contrasts with the effects of modifying attenuation lengths, which would mostly affect sensitivity at high energies. These effects are illustrated by Table III. The Stecker and Salamon AGN model (a), for example, produces events at lower energy, and is seen to be most sensitive to changes in signal strength and sensitivity, whereas the topological defect (d) and GZK (e) models extend to higher energy and are more sensitive to uncertainty in λ_{att} .

To account for the LPM effect, the RICE Monte Carlo uses the parameterization of Ref. [46], which describes a narrowing of the Cherenkov cone due to a lengthening of the shower. The radiation pattern is based on an average shower profile, whereas fluctuations in longitudinal development could lead to “non-gaussian” tails for the angular pattern, which would enhance the effective volume. In addition, the parameterization is developed in the Fraunhofer regime, valid for $R \gg l^2/\lambda$, where R is the distance to the observer, l is the

Group	Item	\pm
Event Generator (Sec. III A)	$\sigma_{\nu N}$	20%
	$(1 - y)$	< 5%
EM pulse (Sec. III B)	shower simulation	10% ^a
	spectrum	10% ^b
	extrapolation: TeV \rightarrow PeV	5%
	LPM effects	See text.
Propagation (Sec. III C)	attenuation $\nu < 1$ GHz	+0.3/-0.15 dB/100 m ^c
	attenuation $\nu > 1$ GHz	^d
	index of refraction	< 1%
	reflections	small
Antenna and DAQ (Sec. III D)	overall channel response	3 dB
	overall channel timing	25/50 ns ^e
	on-line filter efficiency	5%
	dead time	< 5%
Analysis (Secs. III E, IV)	V_{eff}	8% ^f
	nearby vertex reconstruction	10 m ^g
	far vertex reconstruction	0.1 R ^h
	efficiency of analysis chain	5%

^aPulse amplitude

^bFor RICE bandpass of 200-500 MHz

^cThis corresponds to a factor of two uncertainty in λ_{att} .

^dNot critical given bandwidth limitations of antennas, cables, amps, and DAQ elements.

^e25 ns for neutrino events. 50 ns for surface generated noise.

^fStatistical: the Monte Carlo runs produce roughly 150 detections in each E_s bin.

^gw/ assumed 50 ns pulse timing uncertainty, appropriate for noise rejection.

^hw/ assumed 50 ns pulse timing uncertainty, appropriate for noise rejection.

TABLE II: Estimates of systematic effects for different components of the RICE analysis.

shower length, and λ is the wavelength of the radiation. As l increases with the LPM effect, a more accurate treatment will lead to a broader radiation pattern[48, 49], which may enhance the effective volume for high energy showers.

B. Additional event types and hadronic showers

We have restricted our main analysis to electromagnetic showers produced in charged current events of electron neutrinos. The reason for this is two fold: a) simplicity, and b) this process is better studied in the literature. Even so, expanding the analysis to include neutral currents and other neutrino flavors may be expected to increase the rate of neutrino interaction candidates by a factor of 4.5. There is a 50% increase due to including neutral

Model	Nom	2S	0.5S	$2\lambda_{att}$	$0.5\lambda_{att}$
(a)	0.0120	0.0433	0.0023	0.0220	0.0056
(b)	0.1384	0.2597	0.0572	0.3062	0.0526
(c)	0.0050	0.0079	0.0025	0.0118	0.0017
(d)	0.0182	0.0239	0.0123	0.0494	0.0059
(e)	0.0015	0.0021	0.0009	0.0037	0.0005

TABLE III: Expected number of events during a 333.3 hr exposure for different models and assumptions about systematic uncertainties. Models are labeled as in Fig. 8. “Nom” refers to the nominal case used for generating Fig. 8. “2S” and “0.5S” reflect the change in event rate if the signal strength were doubled or halved. “ $2\lambda_{att}$ ” and “ $0.5\lambda_{att}$ ” show the result due to doubling or halving the attenuation length.

Restriction	Effect of relaxation ^a
$\theta_z > 90$ deg	Increase rates 10% ^b
no hadronic shower in ν_e charged current events	0-100% ^c
CC events only	+ 50% per flavor
ν_e events only	$\times 3$
τ decay not included	increase by 1 charged current channel for $E < 20$ PeV
τ regeneration not included	increased event rate for upward neutrinos

^aEstimates are made at $E_{\nu_e} = 1$ EeV, unless stated, where signal from hadronic shower and EM shower are comparable (see Figure 10).

^bThe Earth is not totally opaque just below the horizon, so rates increase slightly, even at high energies.

^cdepends strongly on energy and geometry.

TABLE IV: Summary of event type and geometry considerations in RICE analysis.

currents and a factor of 3 for including all flavors. Additional increases may occur if we include upward neutrinos from just below the horizon and extra efficiency for ν_τ due to regeneration in propagation through the Earth and τ decay in the ice near the RICE array. Table IV summarizes restrictions we have placed on our analysis, and the potential effect on event rates if the restriction were removed.

As described in Section III A the hadronic energy is typically a quarter of that available on the leptonic side of an event. Most of the energy ends up as electromagnetic energy, primarily through π^0 decay; however, that process is not effective until the average pion energy drops below ~ 6 PeV, similar to the energy where LPM effects start to have a significant effect on the longitudinal evolution of the shower. As a result, hadronic showers, although decreased and more variable in energy, do not suffer the decrease in solid angle acceptance for electromagnetic showers related to the LPM effect.

Given the potential importance of hadronic showers, we have recalculated the RICE effective volume under the assumption that LPM effects may be ignored - i.e. the signal

strength scales linearly with shower energy and the angular pattern is energy independent. The result is shown in Figure 10. From the Figure, one may infer that the hadronic shower provides a stronger radio Cherenkov signal than the electromagnetic shower for neutrino energies above ~ 1 EeV, for typical charged current ν_e events.

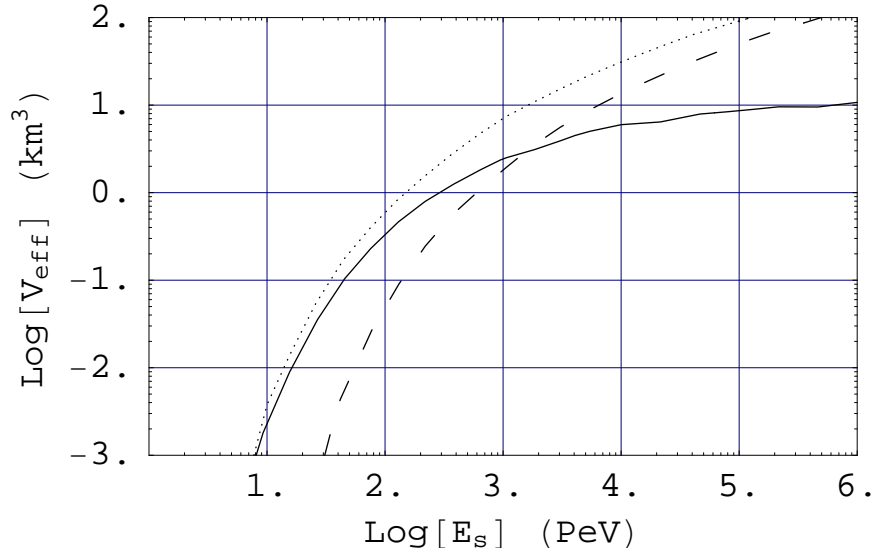


FIG. 10: Effective volume with and without the LPM effect. The solid curve is the same nominal result with LPM shown in Figure 5. The dotted curve shows V_{eff} calculated without the LPM effect. The dashed curve shows the non-LPM result, but shifted in energy by a factor of 4. This roughly mimics the relative response of RICE to hadronic showers (as compared to electromagnetic showers from the same energy neutrino), where the average inelasticity is $\langle y \rangle = 0.2$.

It is now straight forward to replicate the main analysis, with appropriate modifications, to study the potential improvement in sensitivity to be gained by considering hadronic showers produced in charged and neutral currents of all neutrino flavors. These modifications include production of hadronic showers with energy $E_s = yE_\nu$ as outlined in Section III A, and use of the “no-LPM” V_{eff} shown as the dotted curve in Figure 10.

There are three nominal choices to make for the neutrino flavor content, which all lead to the same event rates. If there is no mixing, the flavor content is determined by the physics of π -decay, which yields the well known relation $\phi_{\nu_\mu} \approx 2\phi_{\nu_e}$. If there is mixing amongst ν_μ and ν_τ as suggested by the SuperKamiokande atmospheric neutrino analysis[69], but not ν_e , then the event rate of hadronic showers is unchanged, since ν_μ and ν_τ produce the same hadronic showers at these energies. If there is full mixing of all flavors, then the rate of EM showers is unchanged since the 2 : 1 flavor ratio ($\nu_\mu + \nu_\tau : \nu_e$) at production is unchanged by mixing. For any of these scenarios, Table V gives event rates including hadronic events. For the lower energy AGN models, including hadronic events increases the event rate by factors of 2-4. For the GZK (e) and topological defect (d) models, the increase is significantly larger - 7 and 16 respectively.

Model	ν_e EM	ν_e H	$\nu_\mu + \nu_\tau$ H	Total
(a)	0.0120	0.0049	0.0098	0.0268
(b)	0.1384	0.1096	0.2193	0.4673
(c)	0.0050	0.0063	0.0126	0.0238
(d)	0.0182	0.0962	0.1923	0.3067
(e)	0.0015	0.0029	0.0057	0.0100

TABLE V: Expected number of events during a 333.3 hr exposure for different models, including hadronic showers. Models are labeled as in Fig. 8. “ ν_e EM” is the nominal event rate shown in Fig. 8 for our main analysis. “ ν_e H” gives the event rate due to the hadronic recoil showers from ν_e charged current and neutral current events. Similarly, “ $\nu_\mu + \nu_\tau$ H” gives the event rate due to μ and τ neutrinos. For an isoflavor model this is just twice the ν_e H rate. “Total” gives the sum of the three contributions, as appropriate for either an isoflavor model or a conventional source model with no mixing and $\phi_{\nu_\mu} \approx 2\phi_{\nu_e}$.

We have not modeled τ decay events. To be observed, the τ would have to decay within a km or so of its production site, corresponding to $E_\tau \approx 20$ PeV. Thus, charged current ν_τ events presumably contribute an event rate comparable to the other terms in the Table, but which is suppressed at high energy by the probability $P \sim \frac{20\text{PeV}}{E+20\text{PeV}}$ for the τ to decay in the ice. A proper estimate of this term requires a separate Monte Carlo to deal with the stochastic nature of τ decay. Also, since we confine our analysis to the downward flux of neutrinos, we do not allow for the detection of an upward flux of regenerated ν_τ [70], or ν_e and ν_μ produced in τ decay[71]. Except near the horizon, these are expected to be of fairly low energy compared to the main RICE sensitivity.

VIII. SUMMARY AND OUTLOOK

Using data from the RICE antenna array collected during August 2000, we have searched for nanosecond radio pulses resulting from neutrino interactions in ice. We find no such events, which provides the basis for the diffuse flux limits on ultra-high energy electron neutrinos shown in Figure 8 and Figure 9. This is the primary result of this paper. At the same time, we have demonstrated the efficacy of techniques designed to eliminate anthropogenic backgrounds and thermal noise.

There are many ways by which either a) the limits we have derived can be improved to the level where they seriously constrain models, or b) the experiment results in actual UHE neutrino detection. The most obvious of these is to increase the exposure and validate sensitivity to hadronic showers. Archived data presents a potential increase of more than an order of magnitude increase in exposure. Based on the estimates in Table V, including hadronic cascades would increase the event rates for typical AGN models by factors of 2-4, and by factors as high as 10-15 for GZK and topological defect models. Combined, these factors may achieve a factor of nearly 100 in sensitivity. This would severely test

several models - especially the neutrino fluxes associated with top-down models proposed to explain the purported excess of cosmic rays with energies above the GZK cutoff. It would, however, remain about a decade short of testing the Waxman-Bahcall bound[68] or probing the “guaranteed” flux of neutrinos produced in the GZK process.

To further improve the limits requires improving the acceptance of the experiment by reducing the threshold for event detection, or by increasing the number of antennas and the area over which they are deployed. The main impact of lowering the threshold is to increase the sensitivity at modest energies, 1-100 PeV, but, as illustrated in Figure 5, the gains at higher energy are quite modest. As signal attenuation determines the “horizon” for a single antenna, to improve the RICE sensitivity for energies in excess of an EeV requires deployment of antennas over a wider area.

There are a number of technological improvements that could dramatically improve the sensitivity for energies below 100 PeV, including making use of correlated cross-polarized antennas, increasing the bandwidth, making use of matched filters to maximize signal to noise, and deploying larger numbers of antennas to increase the likelihood that the Cherenkov cone from a true neutrino would intersect four or more antennas.

To ensure that the experiment remains signal limited (as opposed to background limited) the current noise event rejection must be improved without significant loss of efficiency for neutrino events. This should be achievable by simple strategies. For example, increasing the number of antenna hits required in coincidence from 4 to 5, results in more than a hundredfold reduction in thermal noise events, but only a $\sim 15\%$ reduction in neutrino induced events. Similarly, a modest increase in the restrictions of the on-line veto or the analysis cuts on event reconstruction, would reduce impulsive backgrounds significantly without significant reduction in neutrino detection efficiency.

Judging by the summary in Table II, uncertainties associated with RICE need to be reduced as well. Most important is the need for a better determination of the radio attenuation length in ice. We believe the current treatment of λ is on the conservative side by some 30%-50%, which would potentially increase V_{eff} by a factor ~ 2 for $E_\nu > 1$ EeV. Similarly, we believe the parameterization of the LPM effect taken from Ref. [46] may lead to an underestimate of V_{eff} .

Finally, we look forward to the time when true neutrino events are detected by RICE, at which point critical issues will turn from acceptance and noise rejection to the ability to reconstruct events and identify sources and neutrino flavor on an event by event basis. To that end we are improving the timing analysis needed for event reconstruction. Improving the amplitude calibration is critical here as well, since signal strength plays a role in reconstruction of the Cherenkov cone.

To summarize, we believe the outlook for RICE, and the radio Cherenkov technique in general, is quite bright. Analysis of data already in hand should significantly improve present limits on ν_e fluxes. Inclusion of other flavors and interaction modes will further constrain models. We expect the experiment to remain signal limited, not background limited, at least down to levels where even conservative flux models may be observed. The ability to reconstruct the vertex and incident neutrino direction should permit searches for point sources. Similarly, arrival times are sufficiently resolved to conduct coincidence studies between RICE events and gamma-ray bursts. Finally, we expect that the technique should

be extendable to place new limits on “light” relativistic magnetic monopoles[72], as well as neutrino interactions, including production of micro black holes[73, 74, 75, 76].

Acknowledgments

We gratefully acknowledge the generous logistical support of the AMANDA Collaboration (without whom this work would not have been possible), the National Science Foundation Office of Polar Programs, the University of Kansas General Research Fund and the University of Kansas Research Development Fund, the Kansas Center for Advanced Scientific Computing (kasc) and the associated NSF-MRI grant for the support of the KU Origin2400 supercomputer, the NSF EPSCoR Program, the University of Canterbury Marsden Foundation, and the Cottrell Research Corporation. Matt Peters of the U. of Texas SOAR group provided essential consultation on antenna design, calibration and electrical engineering. The National Science Foundation’s Research Experience for Undergraduates Program provided support for Jeff Allen (Shawnee Mission South High School, currently at U. of California, Berkeley), Eben Copple (KU. Physics Dept.), Karl Byleen-Higley (Lawrence High School, Lawrence, KS), Adrienne Juett (KU Physics Dept., currently at MIT), and James Snow (Eudora High School, Eudora, KS), who performed invaluable software assistance and antenna and amplifier calibration. Alexey Provorov and Igor Zheleznykh (Moscow Institute of Nuclear Research) constructed the TEM horn antennas currently used in the surface-noise veto. We also thank the winterovers who staffed the experiment during the last three years at the South Pole (Xinhua Bai, Allan Baker, Mike Boyce, Marc Hellwig, Matthias Leupold, Karl Mueller, Katherine Rawlins, Steffen Richter, and Darryn Schneider.) Ryan Dyer helped in deployment during the 1999-2000 campaign. Very useful conversations with Peter Gorham, Jaime Alvarez-Muñiz, and David Saltzberg are also appreciated and acknowledged. We are indebted to Dan DePardo and Dilip Tammana (University of Kansas Remote Sensing Lab) for their help in setting up and operating the KU Antenna Testing Range, and Alan Hase and Bruce Janus (University of Kansas Dept. of Physics) for their superb machine shop work. We also thank Checkers Supermarket of Lawrence, KS for allowing use of their vegetable freezer as an environmental testing chamber.

-
- [1] T.K. Gaisser, F. Halzen, & T. Stanev, *Phys. Rep.* 258, 173 (1995).
 - [2] IceCube: <http://icecube.wisc.edu/>.
 - [3] F. Montanet [Antares Collaboration], *Nucl. Phys. (Proc. Suppl.)* 87, 436 (2000).
 - [4] NEMO: nemoweb.lns.infn.it/project.htm.
 - [5] P. Greider [NESTOR Collaboration], *Nucl. Phys. Proc. Suppl.* 97, 105 (2000).
 - [6] F. Halzen et al. [AMANDA Collaboration], in *Proceedings of the 26th International Cosmic Ray Conference (ICRC 99)*, Salt Lake City, 17-25 Aug. 1999, B. L. Dingus, D. B. Kieda, M. H. Salamon (Eds.), (AIP, 2000) pp. 428-431 (2000).
 - [7] V. Balkanov et al. [Baikal Collaboration], *astro-ph/0112446* (2001).

- [8] S. Yoshida et al. [AGASA Collaboration], in Proc. 27th International Cosmic Ray Conference, Hamburg, Germany, 2001, Vol. 3, p 1142. (2001).
- [9] M. Lawrence, et al., J. Phys. G 17, 733 (1991); M.Ave et al., Astropart. Phys. 14, 109-120 (2000).
- [10] D. Bird et al. [Fly's Eye Collaboration], Ap. J. 441, 151 (1995); J. Matthews et al. [HiRes Collaboration], in Proc. 27th International Cosmic Ray Conference, Hamburg, Germany, 2001, Vol. 1, p. 350.
- [11] K. Greisen, Phys. Rev. Lett. 16, 748 (1966); G.T. Zatsepin & V.A. Kuzmin, JETP Lett. 4, 78 (1966).
- [12] V.S. Berezhinsky & G.T. Zatsepin, Phys. Lett. 28b, 423 (1969); Sov. J. Nucl. Phys. 11, 111 (1970).
- [13] R. Engel, D. Seckel, & T. Stanev, Phys. Rev. D64, 093010 (2001).
- [14] D. Zavrtanik [AUGER Collaboration], Nucl. Phys. Proc. Suppl. 85, 324 (2000);
- [15] K.S. Capelle, J.W. Cronin, G. Parente & E. Zas, Astropart. Phys. 8, 321-328 (1998).
- [16] OWL: <http://owl.gsfc.nasa.gov/> (2002).
- [17] EUSO: <http://www.ifcai.pa.cnr.it/~EUSO/> (2002).
- [18] N. G. Lehtinen, S. Adam, G. Gratta, T. Berger and M. Buckingham, Astropart. Phys. 17, 279 (2002).
- [19] M.A. Markov & I.M. Zheleznykh, Nucl. Instrum. Meth. A248 242-251 (1986).
- [20] I.M. Zheleznykh, in *Proceedings of Neutrino Neutrino 88: 13th International Conference On Neutrino Physics And Astrophysics* (5-11 Jun 1988), Boston, Massachusetts, Ed. J. Schneps, T. Kafka, W. A. Mann, P. Nath. Teaneck, N.J., World Scientific (1989).
- [21] For a collection of recent contributions see, *First International Workshop on Radio Detection of High-Energy Particles* (RADHEP2000), Los Angeles, 16-18 Nov. 2000. D. Saltzberg and P. Gorham, eds. AIP Conf. Proc. 579 (2001).
- [22] G.A. Askaryan, Zh. Eksp. Teor. Fiz. 41, 616 (1961); G.A. Askaryan, Soviet Physics JETP 14, 441 (1962).
- [23] D. Saltzberg, et al., Phys. Rev. Lett. 86, 2802-2805 (2001).
- [24] P.W. Gorham, K.M. Liewer & C.J. Naudet, HE 6.3.15, Proceedings 26th Int. Cos. Ray Conf., Salt Lake City (1999).
- [25] P.W. Gorham et al., First International Workshop on Radio Detection of High-Energy Particles (RADHEP2000), Los Angeles, 16-18 Nov. 2000. D. Saltzberg and P. Gorham, eds. AIP Conf. Proc. 579, 177-188 (2001).
- [26] P. Gorham, et al., hep-ex/0108027 (2001).
- [27] G. M. Frichter, J. P. Ralston & D. W. McKay, Phys. Rev. D53, 1684 (1996).
- [28] P. Gorham, Presentations at First International Workshop on Radio Detection of High-Energy Particles (RADHEP2000), Los Angeles (2000) and Ultra High Energy Particles from Space, Aspen (2002); (http://www.phys.hawaii.edu/~gorham/Radhep_Aspen.pdf).
- [29] S. Razzaque, et al., Phys.Rev. D65, 103002 (2002).
- [30] S. Razzaque, S. Seunarine, D. Besson, D. McKay, J. Ralston, and D. Seckel in preparation (2003).
- [31] I. Kravchenko, et al., astro-ph/0112372, submitted to Astropart. Phys. (2001).

- [32] G. Frichter, et al., HE 6.3.12, Proceedings 26th Int. Cos. Ray Conf., Salt Lake City (1999).
- [33] D. Seckel, et al., Proceedings 27th Int. Cos. Ray Conf., Hamburg (2001).
- [34] R. Gandhi, C. Quigg, H. Reno & I. Sarcevic, *Astropart. Phys.* 5, 81 (1996).
- [35] R. Gandhi, C. Quigg, H. Reno & I. Sarcevic, *Phys. Rev. D* 58 (093009) (1998).
- [36] G. M. Frichter, D. W. McKay and J. P. Ralston, *Phys. Rev. Lett.* 74, 1508 (1995)
- [37] M. Glück, E. Reya & A. Vogt, *Eur. Phys. J. C* 5, 461 (1998).
- [38] M. Glück, S. Kretzer, & E. Reya, *Astropart. Phys.* 11, 327 (1999).
- [39] J. Kwiecinski, A.D. Martin, & A.M. Staso, *Phys. Rev. D* 59, 093002 (1999).
- [40] NMC Collaboration, P. Amaudruz et al., *Z. Phys. C* 51, 387 (1991); *Z. Phys. C* 53, 73 (1992); *Phys. Lett. B* 295, 195 (1992); NMC Collaboration, M. Arneodo et al., *Nucl. Phys. B* 441, 12 (1995).
- [41] E665 Collaboration, M.R. Adams et al., *Phys. Rev. Lett.* 68, 3266 (1992); *Phys. Lett. B* 287, 375 (1992); *Z. Phys. C* 67, 403 (1995).
- [42] J.A. Castro Pena, G. Parente & E. Zas, *Phys. Lett. B* 507, 231-235 (2001).
- [43] S.I. Dutta et al., *Phys. Rev. D* 63, 094020 (2001).
- [44] J. Alvarez-Muñiz & E. Zas, *Phys. Lett. B* 434, 396-406 (1998).
- [45] E. Zas, F. Halzen & T. Stanev, *Phys. Rev. D* 45, 362 (1992).
- [46] J. Alvarez-Muñiz & E. Zas, *Phys. Lett. B* 411, 218-224 (1997).
- [47] J. P. Ralston & D.W. McKay, “Comparing Coherent Microwave Emission from LPM and B–H Electromagnetic Showers,” in *High Energy Gamma Ray Astronomy* (Ann Arbor 1990), *APS Conference Proceedings No. 220* Ed. J. Matthews, AIP NY (1991).
- [48] J. Alvarez-Muñiz, R.A. Vázquez & E. Zas, *Phys. Rev. D* 62, 063001 (2000).
- [49] R.V. Buniy & J.P. Ralston, *Phys. Rev. D* 65, 016003 (2002).
- [50] J. Alvarez-Muñiz, E. Marques, R.A. Vazquez, & E. Zas, astro-ph/0206043 (2002).
- [51] K. Greisen, *Prog. Cosmic Ray Physics* 3, 1 (1956).
- [52] For an introduction to this difficult subject, see V.V. Bogorodsky, C.R. Bentley and P.E. Gudmandsen, *Radioglaciology*, Riedel, Dordrecht, Holland (1985).
- [53] T.E. Kelihier & S.F. Ackley, “A comparison between derived internal dielectric properties and radio-echo sounding records of the ice sheet at Cape Folger, Antarctica”, Cold Regions Res. and Eng. Lab. (CRREL) Report 78-4, Hanover, NH (1978).
- [54] A. Provorov, Private Communication. The parameterization is based on data given by Bogorodsky and Gavrilov.
- [55] T. Matsuoka, S. Fujita, & S. Mae, *J. Appl. Phys.* 80, 5884 (1996).
- [56] Apparently unpublished, the Westphal data is referred to by S. Evans & B.M.E. Smith, *J. of Physics E*, 2 (1969), Ref. [55], the University of Texas Institute of Geophysics (M. Peters, private communication), the ANITA collaboration (P. Gorham, private communication). The “Iceland” data referred to in Ref. [52] yields essentially identical λ_{abs} , and we suspect may also be due to Westphal.
- [57] S. Kawada, *J. Phys. Soc. Japan* 44, 1881 (1978).
- [58] M.P. Tonkonogov, *Physics Uspekhi* 41, 25 (1998); Tonkonogov et al., *Izv. Vyssh. Uchebn. Zaved., Fiz* (10) 72 (1986).
- [59] S. Fujita, T. Matsuoka, T. Ishida, K. Matsuoka and S. Mae, *Physics of Ice Core Records*, ed.

- T. Hondoh, Hokkaido University Press, Sapporo (2000).
- [60] Frichter, G., reported at the UCI ICECUBE Workshop, UC, Irvine (1998).
 - [61] F.W. Stecker & M.H. Salamon, *Space Sci. Rev.* 75, 341 (1996).
 - [62] R. J. Protheroe, in *Accretion Phenomena and Related Outflows*, IAU Colloquium 163, edited by D. T. Wickramasinghe, G. V. Bicknell and L. Ferrario, ASP Conference Series, V. 121, p. 585 (1997).
 - [63] K. Mannheim, *Astropart. Phys.* 3, 295 (1995).
 - [64] R.J. Protheroe & T. Stanev, *Phys. Rev. Lett.* 77, 3708-3711 (1996); *ibid.* 78, 3420 (1997).
 - [65] S. Yoshida et al. [AGASA Collaboration], in *Proc. 27th International Cosmic Ray Conference*, Hamburg, Germany, 2001, Vol. 3, p 1146. (2001).
 - [66] R.M. Baltrusaitas, et al. [Fly's Eye Collaboration], *Phys. Rev. D* 31, 2192 (1985).
 - [67] J. Ahrens, et al. [Amanda Collaboration], submitted to *Phys. Rev D*, astro-ph-0206487, (2002).
 - [68] E. Waxman & J. Bahcall, *Phys. Rev. D* 59, 023002 (1999); J. Bahcall & E. Waxman, *Phys. Rev. D* 64, 023002 (2001).
 - [69] H. Sobel for the Superkamiokande Collaboration, in *Proceedings of the 19th International Conference on Neutrino Physics and Astrophysics - Neutrino 2000*, Sudbury, Ontario, Canada, 16-21 June, 2000. *Nucl. Phys. Proc. Suppl.* 91, 127-133 (2001).
 - [70] D. Saltzberg and F. Halzen, *Phys. Rev. Lett.* 81, 4305 (1998).
 - [71] J. Beacom, P. Crotty and E.W. Kolb, *Phys. Rev. D* 66, 021302 (2002).
 - [72] S. D. Wick, T. W. Kephart, T. J. Weiler, & P.L. Biermann, astro-ph/0001233, submitted to *Astropart. Phys.* (2001); S. D. Wick, T. W. Kephart and T. J. Weiler, *First International Workshop on Radio Detection of High-Energy Particles (RADHEP2000)*, Los Angeles, 16-18 Nov. 2000. D. Saltzberg and P. Gorham, eds. *AIP Conf. Proc.* 579, 43-52, 2001.
 - [73] J. Alvarez-Muñiz, J.L. Feng, F. Halzen, T. Han, and D. Hooper, *Phys. Rev. D* 65, 124015 (2002).
 - [74] L. Anchordoqui, J. Feng, H. Goldberg and A. Shapere, *Phys. Rev. D* 65, 124027 (2002).
 - [75] M. Kowalski, A. Ringwald and H. Tu, *Phys. Lett. B* 529, 1 (2002).
 - [76] P. Jain, S. Kar, D. Mckay, S. Panda and J. Ralston, *Phys. Rev. D* 66, 065018 (2002).